

**OPEN ACCESS**

## Validation of a vortex ring wake model suited for aeroelastic simulations of floating wind turbines

To cite this article: J B de Vaal *et al* 2014 *J. Phys.: Conf. Ser.* **555** 012025

View the [article online](#) for updates and enhancements.

### You may also like

- [Characterisation of plasma synthetic jet actuators in quiescent flow](#)  
Haohua Zong and Marios Kotsonis
- [A comparative study on the evolution of compressible vortex ring generated from a short driver section shock tube](#)  
Santanu Dey, T Murugan and Dipankar Chatterjee
- [Numerical simulation of head-on collision of two coaxial vortex rings](#)  
M Cheng, J Lou and T T Lim



**ECS**  
The  
Electrochemical  
Society  
Advancing solid state &  
electrochemical science & technology

**DISCOVER**  
how sustainability  
intersects with  
electrochemistry & solid  
state science research

# Validation of a vortex ring wake model suited for aeroelastic simulations of floating wind turbines

J B de Vaal<sup>1,2</sup>, M O L Hansen<sup>2,3</sup> and T Moan<sup>1,2</sup>

<sup>1</sup> Department of Marine Technology, Norwegian University of Science and Technology, Trondheim, Norway

<sup>2</sup> Centre for Ships and Ocean Structures, Norwegian University of Science and Technology, Trondheim, Norway

<sup>3</sup> DTU Wind Energy, Department of Mechanical Engineering, Technical University of Denmark, Lyngby, Denmark

E-mail: [jacobus.b.de.vaal@ntnu.no](mailto:jacobus.b.de.vaal@ntnu.no)

**Abstract.** In order to evaluate aerodynamic loads on floating offshore wind turbines, advanced dynamic analysis tools are required. As a unified model that can represent both dynamic inflow and skewed inflow effects in its basic formulation, a wake model based on a vortex ring formulation is discussed. Such a model presents a good intermediate solution between computationally efficient but simple momentum balance methods and computationally expensive but complete computational fluid dynamics models. The model introduced is shown to be capable of modelling typical steady and unsteady test cases with reasonable accuracy.

## 1. Introduction

The objective of this work is to validate a wind turbine wake model, based on vortex rings, with the intention of using the model as an aerodynamics module in an aeroelastic simulation of floating offshore wind turbines (FOWTs). FOWTs operate in a highly dynamic environment (wind and wave) and since they are mounted on floating platforms, the rotor will experience larger motions compared to a bottom fixed wind turbine rotor. Most commonly used aeroelastic load analysis tools developed and validated for use on bottom fixed wind turbines rely heavily on quasi-steady momentum balance equations coupled with engineering models to account for dynamic effects. Due to larger aerodynamic unsteadiness experienced by FOWTs, methods including more flow physics than the quasi-steady momentum balance based ones, may in certain cases be required to adequately analyse dynamic loads.

Compared to blade element and momentum theory (BEMT) models, a free wake vortex ring (VR) model includes more flow dynamics inherently, but at a larger computational cost. It is, however, still significantly more computationally efficient than the axisymmetric actuator disc (AD) model - an even more physically complete model. The VR model is an intermediate solution, and as such an attractive approach for the analysis of a FOWT.

The unsteady motions experienced by an FOWT are largely determined by the topology of the floating platform. Motions that are likely to influence unsteady aerodynamic loads are pitch for a barge, pitch and yaw for a spar-buoy, and surge and pitch for a tension leg platform [1]. This highlights the need for an aerodynamic model that is capable of correctly modelling skewed and sheared flows. BEMT models rely on corrections from engineering models in case of skewed



flow. A VR model can include skewed flow effects in a simplified manner [2], while retaining the advantage over the BEMT method of built-in dynamic flow development.

In this paper, the VR model and the theory it is based on is discussed in some detail, after which comparisons are made to BEMT and AD calculations for representative steady and dynamic cases in order to evaluate the performance of the VR model.

## 2. Vortex ring theory

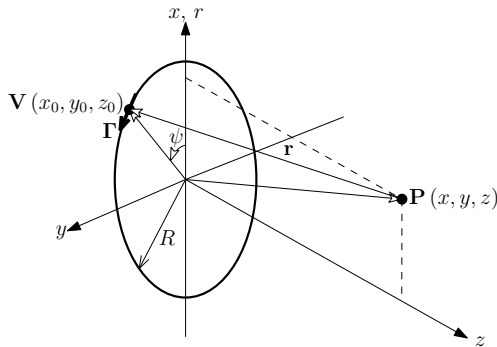


**Figure 1.** Geometry for defining the velocity induced at a field point by a vortex ring located in the  $xy$ -plane.

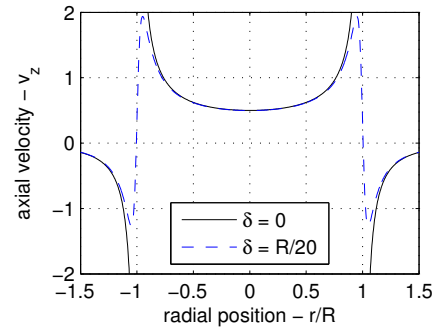


**Figure 2.** Induced velocity in the plane of a vortex ring of unit  $\Gamma$ , with and without the regularisation parameter  $\delta$ .

The velocity induced at a control point,  $\mathbf{P}$ , by a vortex ring of radius,  $R$ , located in the  $xy$ -plane, can be obtained by integrating the Biot-Savart law describing the velocity induced by a vortex filament of strength,  $\Gamma$ , over one rotation along the azimuth  $\psi$  [3].

$$\mathbf{u} = \oint \frac{\mathbf{r} \times \mathbf{\Gamma}}{4\pi|\mathbf{r}|^3} \quad (1)$$

where,

$$\mathbf{r} = \mathbf{V} - \mathbf{P} = [R \cos \psi - r, R \sin \psi, -z] \quad \text{and} \quad \mathbf{\Gamma} = \Gamma d\mathbf{l} = \Gamma[-R \sin \psi, R \cos \psi, 0]d\psi \quad (2)$$

The resulting solution is, however, singular in case the evaluation point  $\mathbf{P}$  falls on the ring itself; that is if  $z = z_0$  and  $r = R$ . To overcome the singular behaviour, a regularisation parameter  $\delta$  representing a vortex with a finite core thickness can be introduced [4]. This entails modifying equation (1) to

$$\mathbf{u} = \oint \frac{\mathbf{r} \times \mathbf{\Gamma}}{4\pi(|\mathbf{r}|^2 + \delta^2)^{3/2}} \quad (3)$$

After some manipulation, equation (3) can be evaluated to give the following de-singularised expressions for the radial and axial induced velocities in terms of complete elliptic integrals of the first ( $K(m)$ ) and second kind ( $E(m)$ )

$$u_r^\delta = \frac{\Gamma}{2\pi a} \frac{z}{r} \left[ \frac{(r^2 + R^2 + z^2 + \delta^2)}{A} E(m) - K(m) \right] \quad (4)$$

$$u_z^\delta = \frac{\Gamma}{2\pi a} \left[ \frac{-(r^2 - R^2 + z^2 + \delta^2)}{A} E(m) + K(m) \right], \quad (5)$$

where

$$A = (r - R)^2 + z^2 + \delta^2, \quad a = \sqrt{(r + R)^2 + z^2 + \delta^2} \quad \text{and} \quad m = \frac{4rR}{a^2}. \quad (6)$$

### 3. Vortex ring model for a wind turbine wake

An idealised model of a wind turbine wake is introduced where the induced velocities on the rotor plane are determined by modelling the influence of the cylindrical vortex tube that forms behind the rotor in discretised form using thin cored vortex rings. By considering the rotor blades as a lifting lines with constant strength,  $\Gamma$ , vorticity is only trailed from the root and the tip of each blade. For an infinite number of blades, the tip vortices will form a continuous cylindrical vortex sheet behind the rotor, whereas the root vortices will combine to form a single vortex along the rotor axis. Since the root vortex is primarily responsible for inducing rotational velocity in the vortex wake; as a first approximation this component will be neglected.

#### 3.1. Relating thrust, induced velocity and vortex strength

The objective of this model is to relate the thrust force  $T$  on the rotor to the vorticity density  $\gamma$  in the wake and the axial velocity  $w_z$  that this induces in the rotor plane. The following steps, based on [5, 6, 7, 8], will indicate how this can be done. Refer to Figure 3 for the notation used in the derivation.

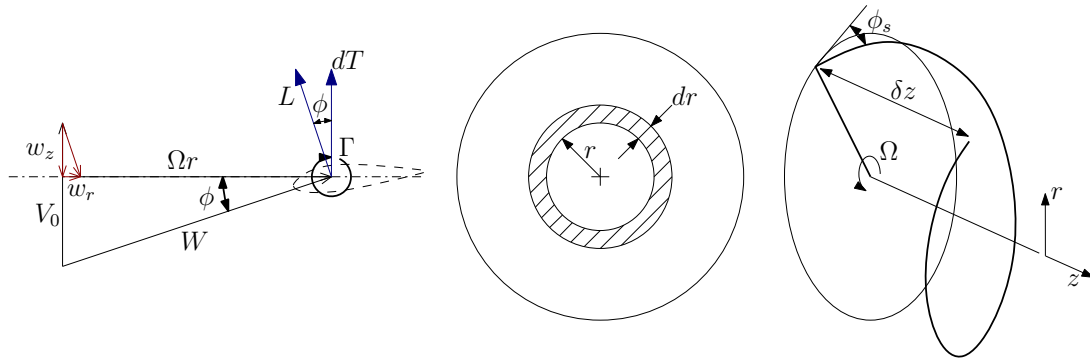


**Figure 3.** Velocity and force vectors on a blade element as seen in the rotor plane (left), an annular element on the rotor for which it applies (middle) and the tip vortex shed from a blade that forms the wake (right).

The axial force on an elemental length  $dr$  along a blade can be related to the bound circulation through the Kutta-Joukowski theorem, according to which  $L = \rho W \Gamma$ , so that

$$dT = \rho(w_r + \Omega r)\Gamma dr \approx \rho\Omega r\Gamma dr \quad (7)$$

Since  $\Gamma$  is assumed constant along a blade, equation (7) can be integrated over the rotor radius and summation for all  $B$  rotor blades gives the total thrust force as

$$T = 0.5\rho V_0^2 \pi R^2 C_T = 0.5\rho\Omega R^2 \Gamma B, \quad (8)$$

which gives

$$\Gamma = \frac{\pi V_0^2 C_T}{\Omega B} \quad (9)$$

The vorticity density  $\gamma$  in the wake is determined by equally distributing the shed vorticity  $\Gamma$  over a distance  $\delta z$  - the distance over which it is transported until another blade passes. This distance is found by considering the time,  $\Delta t$ , between blade passings

$$\Delta t = \frac{2\pi}{\Omega B} = \frac{\delta z}{(V_0 - w_z)} \Rightarrow \delta z = \frac{2\pi(V_0 - w_z)}{\Omega B}, \quad (10)$$

assuming the vortex is transported at the same velocity as that at the disc,  $(V_0 - w_z)$ . Furthermore, the helix angle at which the tip vortex is shed is given by

$$\phi_s = \tan^{-1} \left( \frac{V_0 - w_z}{\Omega R} \right). \quad (11)$$

Only the tangential component of the vorticity density,  $\gamma_t$ , is responsible for inducing axial velocities at the rotor plane so that

$$\gamma_t \delta z = \Gamma \cos \phi_s \quad (12)$$

At radius  $r = R$ , the inflow and helix angles are equal, so that  $\cos \phi_s = \frac{\Omega R}{W}$ . Combining this with equations (9), (10) and (12) then gives

$$\gamma_t = \frac{\pi V_0^2 C_T}{\Omega B} \frac{\Omega R}{W} \frac{\Omega B}{2\pi(V_0 - w_z)} = \frac{V_0^2 C_T}{2(V_0 - w_z)} \frac{\Omega R}{W} \quad (13)$$

### 3.2. Unsteady wake model

In the unsteady model considered, each wake segment of length  $dz$  is represented by a vortex ring. The coupled nature of the problem (vortex ring strength  $\Gamma_r$  is a function of the induced velocity  $w_z$  but the vortex ring wake also determines induced velocity) is taken into account by modelling the wake development in a transient manner. Every time step  $dt$ , a new vortex ring is formed with its strength determined by the current induced velocity on the rotor. All vortex rings are then convected based on the new induced velocity field. Noting that  $dz = (V_0 - w_z)dt$  the strength of the vortex ring released every time step  $dt$  is given by

$$\Gamma_r = \gamma_t dz = \gamma_t (V_0 - w_z) dt = \frac{V_0^2 C_T}{2} \frac{\Omega R}{W} dt \quad (14)$$

The development of the wake is modelled by considering the induced velocities at two control points on each vortex ring. The control points are located in the same plane with a  $180^\circ$  azimuthal offset from each other. The notation is shown in Figure 4 where the upper control points  $\mathbf{x}$  are indicated by the symbol  $\circ$  and the lower ones by  $\square$ . Both the axial convection and radial expansion of the vortex rings are determined by the induced velocity at the control points. Using a simple forward Euler scheme, the position update scheme is expressed as

$$\mathbf{x}^{t+dt} = \mathbf{x}^t + \mathbf{u}^t dt \quad (15)$$

where the velocities at the control points have been calculated from an influence coefficient matrix,  $\mathbf{A}$ , determined by the current vortex ring wake geometry, and a vector,  $\mathbf{\Gamma}_r$ , of ring vortex strengths

$$\mathbf{u}^t = \mathbf{A}(\mathbf{x}^t) \mathbf{\Gamma}_r^t \quad (16)$$

For improved stability and accuracy, a higher order integration scheme could also be used. However, this would require the influence coefficient matrix to be set-up and velocities evaluated according to equation (16), more than once per time step - which is computationally expensive. In the current work, only the first order method with a sufficiently small time step is used.

### 3.3. Model for skew inflow

A more challenging case to model presents itself when inflow is not perpendicular to the rotor disc. Some further simplifying assumptions can, however, be made to develop a baseline model that captures some of the important effects of skewed inflow. Following the approach originally suggested by [9], the time averaged induced velocity at the disc can be obtained by neglecting the

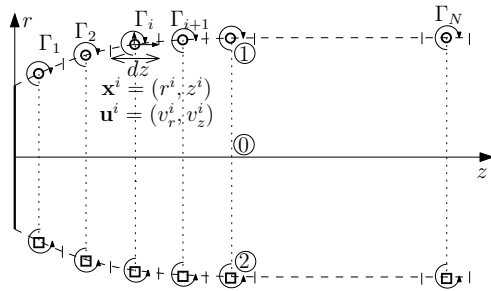


**Figure 4.** Notation used in the free vortex ring wake model.

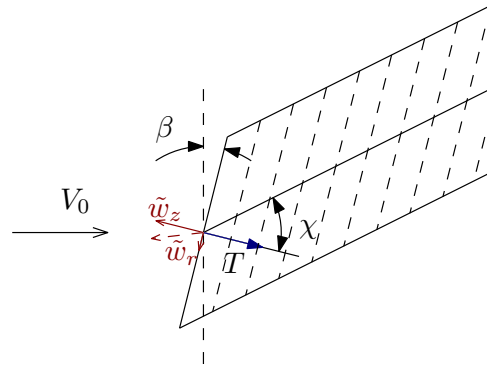


**Figure 5.** Skewed wake that forms due to misalignment between inflow and the actuator disc

azimuthal variation of wake vorticity and still only considering the component of vorticity shed into the wake that is parallel to the rotor disc, see Figure 5. Unlike the axisymmetric problem, in the skewed inflow case control points forming a vortex ring will be convected asymmetrically in a time step. The new positions of the control points will be used to reconstruct the rings each time step. Furthermore, the vortex rings will be at an angle  $\beta$  with respect to the axis of the inertial reference frame. These quantities are determined for the  $i = 1..N$  vortex rings as

$$\begin{aligned} R^i &= 0.5\sqrt{(z_1^i - z_2^i)^2 + (r_1^i - r_2^i)^2} \\ \mathbf{x}_0^i &= 0.5[(r_1^i + r_2^i), (z_1^i + z_2^i)] \\ \beta^i &= \arctan\left(\frac{z_1^i - z_2^i}{r_1^i - r_2^i}\right) \end{aligned} \quad (17)$$

The velocities induced by a vortex ring, equations (4) and (5), apply only in a reference frame local to the ring. It is therefore necessary to convert all control points ( $\mathbf{x}$ ) from the inertial reference frame to the local reference frame of a particular ring ( $\tilde{\mathbf{x}}$ ), to evaluate the induced velocity in the local reference frame, after which the velocities can be converted back into the inertial reference frame.

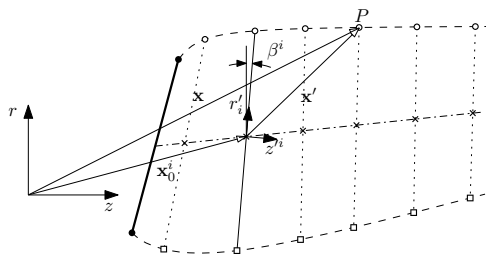


**Figure 6.** Inertial reference frame

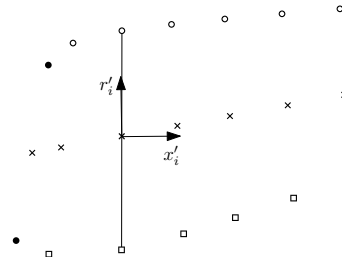


**Figure 7.** Local reference frame

All points of interest are defined in the inertial reference frame ( $r, z$ ) as in Figure 6, while the rotor and each of the vortex rings have a local reference frame ( $r', z'$ ) associated with them. A point in the IRF can thus be described by  $\mathbf{x} = \mathbf{x}_0 + \mathbf{x}'$  or  $\mathbf{x}' = \mathbf{x} - \mathbf{x}_0$ . This coordinate is then transferred into a local reference frame, shown in Figure 7, as  $\tilde{\mathbf{x}} = R_{IL}(\mathbf{x} - \mathbf{x}_0)$ . Once induced

velocities have been determined in the local reference frame,  $\tilde{\mathbf{u}}$ , they are then transformed back into components in the IRF according to  $\mathbf{u} = \mathbf{R}_{LI}\tilde{\mathbf{u}}$ .

### 3.4. Calculation procedure

The wake is initialised with a predetermined number of  $N$  vortex rings, initially with zero strength. In each calculation step, the vortex ring directly behind the rotor is assigned a value based on the current induced velocity. At the end of the time step all the vortex rings are convected according to the induced velocity at their control points, after which their indices are shifted, clearing space for a new ring to be added in the next time step and discarding the  $N^{\text{th}}$  ring. The calculation procedure is outlined below.

- (i) Based on the current values for the induced velocity on the rotor, determine the wake skew angle  $\chi$  and the strength of the first vortex ring behind the rotor - taking into account that  $dz = ds \cos(\chi)$  (where  $ds$  is in the direction of wake propagation)

$$\chi = \frac{V_0 \cos \beta - \tilde{w}_z}{V_0 \sin \beta - \tilde{w}_r} \quad (18)$$

$$\Gamma_r^1 = \frac{C_T V_0^2 \Omega R}{2 W} \cos(\chi) dt, \quad \text{where } W = \sqrt{(V_0 - w_z)^2 + (\Omega R)^2} \quad (19)$$

- (ii) The positions of the two control points defining the vortex ring shed from the rotor is determined from the position of the rotor tips and the velocity vector at the rotor's origin:

$$\begin{aligned} r_1^1 &= r_1^P + (V_0 \sin \beta - \tilde{w}_r) \frac{dt}{2}, & r_2^1 &= r_2^P + (V_0 \sin \beta - \tilde{w}_r) \frac{dt}{2} \\ z_1^u &= z_1^P + (V_0 \cos \beta - \tilde{w}_z) \frac{dt}{2}, & z_2^1 &= z_2^P + (V_0 \cos \beta - \tilde{w}_z) \frac{dt}{2} \end{aligned} \quad (20)$$

- (iii) The influence matrices  $\mathbf{A}_r$  and  $\mathbf{A}_z$  are determined based on the current wake geometry so that the induced velocity at each control point can be determined according to (16).  
 (iv) New positions for the vortex rings are determined according to (15) and the vortex ring size/orientation is updated according to (17).  
 (v) Steps  $i$  to  $iv$  are then repeated for the next time step.

## 4. Simulation results and comparisons

A variety of simulations are performed to test the performance of the vortex ring wake model, and to compare it to commonly used methods based on blade element and momentum theory including engineering corrections, and also a more advanced computational fluid dynamics based actuator disc model.

### 4.1. Steady axial flow

Three different wake configurations are modelled. In the first, a cylindrical vortex tube with a radius equal to that of the rotor is mimicked, where all vortex rings are convected at  $V_0 - w_z$  as measured at the disc. As Figure 8 shows, axial momentum theory is matched nearly identically. Next, the vortex tube radius is again held constant, but the vortex rings forming the tube are allowed to convect in the axial direction according to the local induced velocity. For a given thrust loading, Figure 8 shows that a lower induced velocity is predicted at the disc. This is also the case in the near wake - as a consequence the rings are convected away faster, hence reducing their influence at the disc. Radial expansion is, however, ignored. To correct this inconsistency, the final case considers the full implementation of the model, where rings are convected based

on local velocities in both the axial and radial directions. Even lower induced velocity is now predicted, as rings expand, the velocity induced in the axial direction is reduced, with the effect observed at the rotor disc. The wake expansion for various  $C_T$  is shown in Figure 9. It indicates some break-up of wake surface. This can be compared to the smooth and semi-infinite wake surface modelled in for example [8], that results in somewhat larger wake expansion and higher induced velocities at the rotor disc. The finite wake length will also influence results, although Figure 11 shows that beyond a wake length of approximately  $20R$ , induced velocity at the rotor disc is fairly insensitive to changes in wake length - converging, however, to a value not in complete agreement with axial momentum theory.

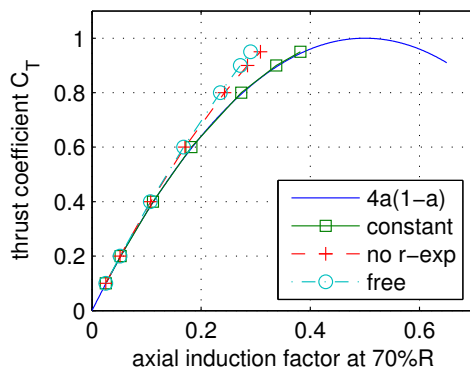


**Figure 8.** Axial induction factor at  $r = 0.7R$  for different wake models and the classical momentum theory.

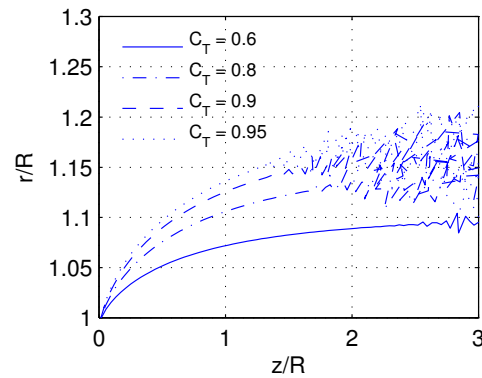


**Figure 9.** The wake expansion at the rotor tip for the free vortex ring wake for different  $C_T$ .

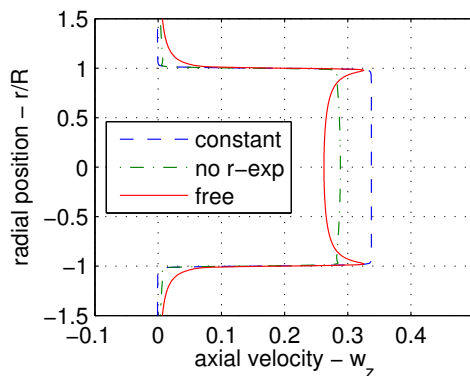


**Figure 10.** Induced velocity profiles on the rotor disc for different wake assumptions. In all cases  $C_T = 0.9$ , with equivalent azimuthal steps of  $20^\circ$  and a wake length of  $20R$ .

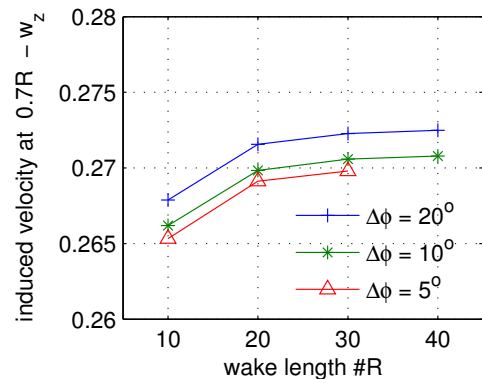


**Figure 11.** Sensitivity of  $w_z$  at  $r = 0.7R$  for various wake discretisation parameters, in all cases  $C_T = 0.9$ , for which axial momentum theory predicts  $w_z = 0.3419$ .

#### 4.2. Steady skewed inflow

In case the rotor is misaligned with the inflow direction, thus in yaw or pitch, there will be an azimuthal variation in induced velocity over the disc - with higher induction on the downstream

side than on the upstream side. Consequently the wake will be distorted, a measure of which is the wake skew angle  $\chi$ , the angle between the wind velocity in the wake and the downstream rotor normal. Figure 12 shows an example of the wake that is formed with the vortex ring model for a rotor in a yawed orientation, giving a good visual representation of the wake skew angle. The magnitude of the wake skew angle is larger than the rotor skew angle, with the difference increasing at an increased thrust coefficient. In Figure 13 the wake skew angle as predicted with the vortex ring model and a yaw model for the BEM method by Glauert [10] are compared to experimental measurements [11]. Although the correct trends are predicted by the vortex ring model, it somewhat under predicts the measured values at higher thrust coefficients.

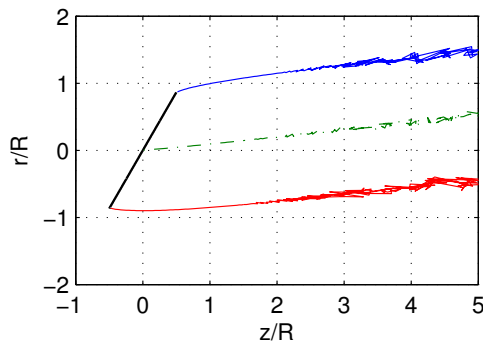


**Figure 12.** The wake behind a rotor at  $C_T = 0.9$  with  $\beta = 30^\circ$  as calculated with the vortex ring code. The midpoints of the vortex rings give an indication of the wake skew angle, while the control points define the wake shape.

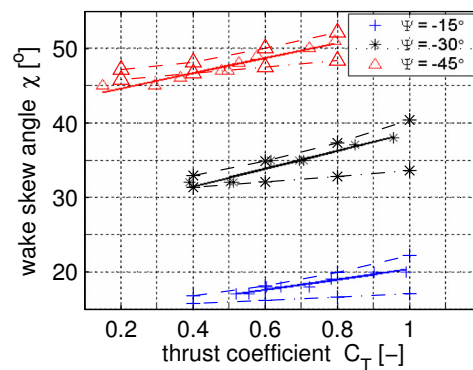


**Figure 13.** Wake skew angle  $\chi$  as function of  $C_T$ , calculated using BEM with yaw correction (---) and with the vortex ring model (— · —), compared to measurements (—). Image adapted from [11].

#### 4.3. Unsteady surge motion

A potential advantage of the vortex ring model, as compared to a blade element momentum theory based method, is its capability to model wake dynamics without the need for additional modelling assumptions. A case of interest is that of a floating wind turbine undergoing comparatively large amplitude and low frequency surge motion due to wave and wind induced loads. Although the effective velocity seen by a blade element is simple to determine, defining the appropriate mass flow through the rotor for use in the BEMT based method is somewhat ambiguous. As a simplified test case, a rotor disc with constant thrust loading will be oscillated at a prescribed frequency, and in this manner the dynamics of induced velocity development with various modelling strategies can be investigated. In the current investigation a commonly used dynamic inflow model by S. Øye, as described in [10], is considered whereby the induced velocity on an annular section of the rotor is modelled by means of two first order differential equations

$$\begin{aligned}
 w_q &= \frac{dT}{4\pi\rho r(V_0 - w_z - u_{surge})} & \tau_1 &= \frac{1.1}{(1 - 1.3a)} \frac{R}{V_0} \\
 w' + \tau_1 \frac{dw'}{dt} &= w_q + 0.6 \cdot \tau_1 \frac{w_q}{dt} & a &= \frac{w_z + u_{surge}}{V_0} \\
 w_z + \tau_2 \frac{dw_z}{dt} &= w' & \tau_2 &= \left[ 0.39 - 0.26 \left( \frac{r}{R} \right)^2 \right] \cdot \tau_1
 \end{aligned} \tag{21}$$

By assuming a constant thrust force, the parameters of the dynamic inflow model are only perturbed by the time dependent surge velocity,  $u_{surge}(t) = u_0 \cos(\omega t)$ . This surge velocity is due to a prescribed axial displacement of the rotor given by  $z_{surge} = z_0 \sin(\omega t)$ , which implies that  $u_0 = \omega z_0$ .

In addition to the dynamic inflow and vortex ring models, a moving actuator disc model is also used to evaluate the induced velocity on an oscillating rotor disc. In this method, blade forces are calculated in the same manner as for the BEMT method, but are now introduced into a flow field as body forces  $\mathbf{f}'$ . The magnitude and position of the body force vector is updated after every time step while solving equation (22) numerically using the commercial software package *FLUENT*.

$$\frac{\partial(\rho\mathbf{v})}{\partial t} + \nabla \cdot (\rho\mathbf{v}\mathbf{v}) = -\nabla p + \nabla \cdot (\bar{\tau}) + \rho\mathbf{g} + \mathbf{f}'. \quad (22)$$

Results for three surge frequencies and amplitude  $z_0 = 0.1R$  are presented in Figures 14 to 16. The average slope of the oscillations show a marginal increase in induced velocity at the rotor

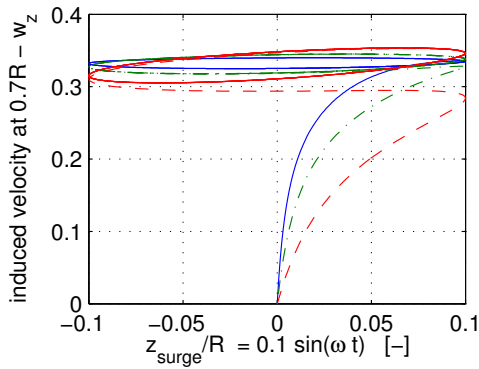


**Figure 14.** Induced velocity according to S. Øye model (21), with  $\omega = 0.1\text{rad/s}$  (—),  $\omega = 0.25\text{rad/s}$  (— · —) and  $\omega = 0.5\text{rad/s}$  (---).

disc as it moves into the wake, and then somewhat lower as it moves into the free-stream and out of the wake. This effect is amplified as the oscillation frequency increases and all models predict similar behaviour. Although the vortex ring model, Figure 15, shows similar dynamic behaviour to the other models, it predicts somewhat lower induced velocity values for a given thrust loading, as alluded to earlier.

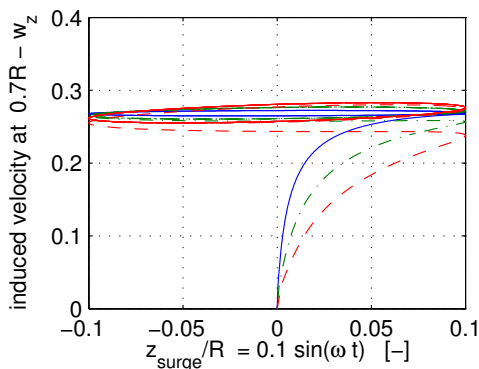


**Figure 15.** Induced velocity calculated using the vortex ring model, with  $\omega = 0.1\text{rad/s}$  (—),  $\omega = 0.25\text{rad/s}$  (— · —) and  $\omega = 0.5\text{rad/s}$  (---).

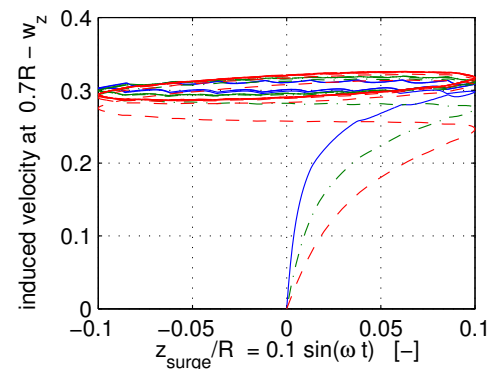


**Figure 16.** Induced velocity according to an actuator disc model, with  $\omega = 0.1\text{rad/s}$  (—),  $\omega = 0.25\text{rad/s}$  (— · —) and  $\omega = 0.5\text{rad/s}$  (---).

## 5. Conclusions

Giving a vortex ring filament a small but finite core size, de-singularises the expressions for (self-)induced velocity, and allows the evaluation of velocity on the vortex ring itself. The convection of such thin cored vortex rings can then be described numerically, making them physically meaningful building blocks to be used in a dynamic rotor wake model. This is done by representing a cylindrical vortex tube in a discretised manner by de-singularised vortex rings. Classical axial momentum theory results can be replicated and more physically correct solutions including wake expansion can be modelled. Although the salient features are captured, the induced velocity calculated at higher thrust coefficients in axisymmetric flow can possibly be improved with more accurate modelling assumptions.

The vortex ring model predicts qualitatively correct wake behaviour for skewed inflow, by only considering the skewed geometry of the wake. The resulting wake skew angle predicted is somewhat lower compared to available measured values. In unsteady surge experiments, the VR model predicts similar dynamic behaviour as a BEMT model with a dynamic inflow model, and an actuator disc computational fluid dynamics model. This emphasises the potential usefulness of the VR for modelling aerodynamics of floating wind turbines, since the dynamics that is built in to its formulation allows it to be applied to a variety of realistic inflow conditions without the need for further explicit modelling of dynamic or skewed inflow effects.

## References

- [1] Sebastian T and Lackner M 2012 *Wind Energy*
- [2] Micallef D, Ferreira C, Sant T and van Bussel G 2010 *Torque 2010 The Science of making Torque from Wind*
- [3] Newman S 2011 The induced velocity of a vortex ring filament Tech. Rep. AFM-11/03 University of Southampton, School of Engineering Sciences
- [4] Saffman P 1992 *Vortex dynamics* (Cambridge University Press)
- [5] Burton T, Sharpe D, Jenkins N and Bossanyi E 2001 *Wind Energy Handbook* (Wiley)
- [6] Johnson W 1994 *Helicopter theory* (New York: Dover Publications)
- [7] Snel H and Schepers J 1995 Joint investigation of dynamic inflow effects and implementation of an engineering method Tech. Rep. ECN-C-94-107 Energy research Centre of the Netherlands Petten
- [8] Øye S 1990 *Proceedings of the third IEA symposium on the aerodynamics of wind turbines, ETSU, Harwell*
- [9] Coleman R, Feingold A and Stempin C 1945 *National Advisory Committee for Aeronautics*
- [10] Hansen M 2008 *Aerodynamics of wind turbines* (Earthscan)
- [11] Haans W, Sant T, Van Kuik G and Van Bussel G 2005 *43th AIAA Aerospace Sciences Meeting and Exhibit* pp 136–145